MUON SCATTERING INTO 1 - 5 MUON FINAL STATES

A.R. Clark, K.J. Johnson, L.T. Kerth, S.C. Loken, T.W. Markiewicz,
P.D. Meyers, W.H. Smith, M. Strovink, and W.A. Wenzel
Physics Department and Lawrence Berkeley Laboratory, University of California, Berkeley, California 94720

R.P. Johnson, C. Moore, M. Mugge, and R.E. Shafer
Fermi National Accelerator Laboratory, Batavia, Illinois 60510

G.D. Gollin, F.C. Shoemaker, and P. Surko
Joseph Henry Laboratories, Princeton University, Princeton, New Jersey 08544

Presented by M. Strovink

Interactions of 209-GeV and 90-GeV muons within a magnetized-steel calorimeter have produced final states containing one, two, three, four, and five muons. Redundant systems of proportional and drift chambers, fully sensitive in the forward direction, maintained 9% dimuon-mass resolution and high acceptance for multimuon final states. We present the first data on $F_2(x, Q^2)$ from charged lepton-nucleon scattering spanning a range in $\ell n\ (\ell n\ Q^2)$ comparable to that measured in high-energy neutrino scattering. The muon data confirm the decrease of F_2 with rising Q^2 in the region $0.2 < x < 0.6$, in agreement with QCD expectations. From >80% of the world sample of fully-reconstructed 3μ final states containing the $J/\psi(3100)$, the first determination of the ψ polarization yields $\sigma_L/\sigma_T = \xi^2 Q^2/m_\psi{}^2$ with $\xi^2 = 4.0\ ^{+5}_{-2}{}^{.4}_{.1}$, 2.6 standard deviations above the vector-dominance expectation. A sample of 35539 two-muon final states contains a small excess of high-$p_\perp$ high-Q^2 same-sign pairs and sets limits on neutral heavy lepton production by right-handed currents. Two five-muon final states are observed, of which only one is the likely result of a pure QED process. A single event with four muons in the final state is interpreted as diffractive $b\bar{b}$ production with $\bar{b} \to \psi X \to \mu^+\mu^- X$ and $b \to \mu^-\bar{\nu}_\mu X$.

During the last two Lepton-Photon Symposia, muon scattering has provided new insight into the constituent structure of hadrons. For example, in 1975 the Cornell-Michigan State-California group[1] reported a rise of F_2 with Q^2 at low x which could not be mitigated by redefinition of x. Subsequently, that effect was widely interpreted as part of the pattern of scale-noninvariance predicted specifically by quantum chromodynamics, amounting to the first experimental support for that theory.

The subtle variations probed by spacelike photons have been overwhelmed in size by the structures due to new flavors revealed by timelike photons. Too little is understood of the spacelike-timelike connection. For example, what effect has the charmed-quark mass on the scale to which F_2 is noninvariant? This report describes early data from the Berkeley-Fermilab-Princeton (BFP) multimuon spectrometer, which integrates precise measurement of inelastic structure-function variations and high sensitivity, through multimuon final states, to flavor thresholds which must contribute to those variations. Following a description of the experiment, data containing one, three, two, five, and four muons in the final state will be presented. Each channel either is detected for the first time, or is observed with unprecedented sensitivity.

Experimental Method

A muon spectrometer of the BFP type was first proposed[2] in 1973. In the Fermilab muon beam the desired luminosity ($\gtrsim 10^6$ nb^{-1} per experiment) is achieved with a massive target ($\sim$5 kg/cm^2). High acceptance over the full target length makes necessary a spectrometer magnet integral with the target. Its steel plates function also as hadron absorbers for calorimetry and muon identification. Computer simulations of multimuon final states underscore the necessity for full acceptance in the forward direction, with no blind "beam hole". Inability to determine the momentum of muons scattered or produced near 0° can remove vital analysis constaints; inability to find all the final state muons can alter drastically the interpretation of many events. A dipole field configuration, requiring only one pair of coils for the full magnet, is most compatible with high forward acceptance. Proportional and drift chambers can withstand the full beam flux at Fermilab (typically 2×10^6 muons per 1-sec spill) without deadening in the beam area. With this design, the spectrometer optimizes and extends the utility of the existing beam.

Construction of the apparatus depicted in Fig. 1 was completed in 1977. It consists of 18 25-ton modules each containing 5 10-cm thick steel plates, 5 calorimeter scintillators (omitted in modules 16-18), and a pair of proportional (PC) and drift chambers (DC). Banks of 12 trigger scintillators (S_1-S_{12}) are located in even modules 4-18. The fiducial volume, 1.8×1 m^2 in area, extends 16 m in the beam direction. Within the central 1.4×1 m^2 area of each magnet plate, the 19.7 kgauss field is uniform to 3% and mapped to 0.2%. Located upstream of module 1 are one additional PC and DC, 63 beam scintillators, 8 beam PC's, and 94 scintillators sensitive to accidental beam and halo muons.

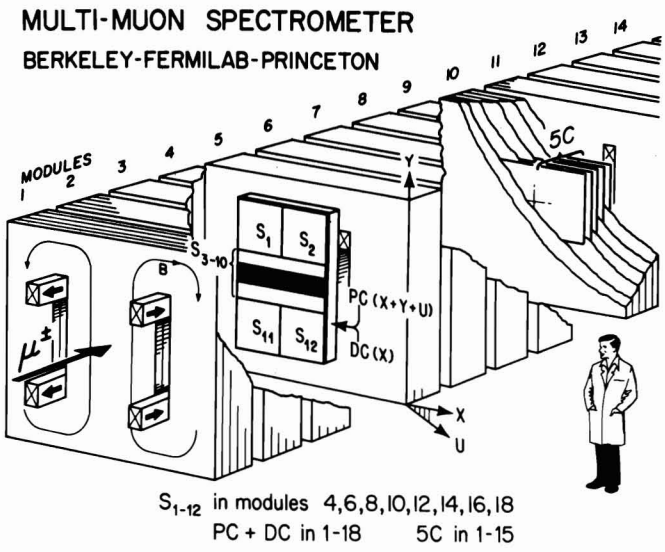

FIG. 1. Schematic view of the apparatus. The solid dipole spectrometer magnet serves also as a target and hadron absorber. S_1-S_{12} are trigger scintillators (1 of 8 banks). DC and PC are 1 of 19 pairs of drift and proportional chambers. Each proportional chamber measures projections on three coordinates. The scintillators labelled 5C are 5 of 75 counters performing hadron-shower calorimetry.

Figure 2 is an exploded view of the detectors in a gap between modules. The 2-cm drift chamber cell and specially designed readout electronics make possible a system efficiency exceeding 98% during high-rate ($\lesssim 10^7$ Hz) conditions[3]. Twofold DC ambiguities are resolved by the PC anode wires, spaced at Δx=3 mm. Coordinates at 30° (u) and 90° (y) to the bend direction (x) are registered in the proportional chambers by means of 5 mm wide cathode strips. Each strip is connected to one input of a differential amplifier in the network

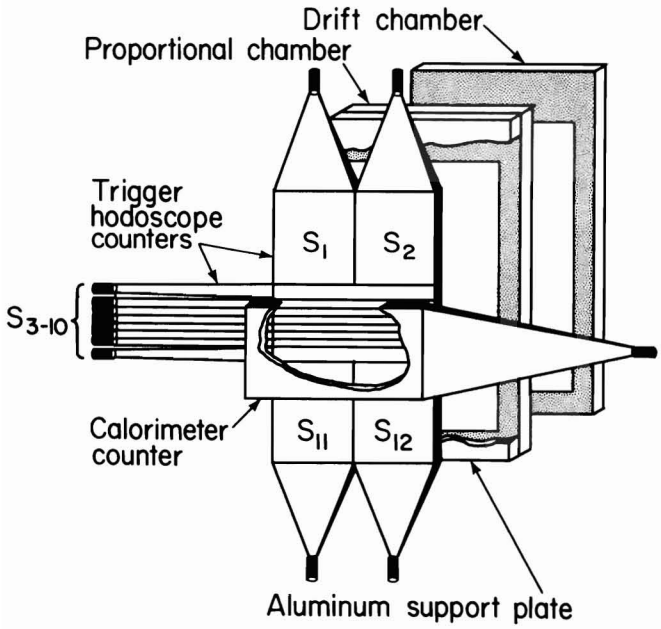

FIG. 2. Exploded view of detectors within a typical gap between magnet modules.

Table 1. Trigger requirements for ≥1μ, ≥2μ, and ≥3μ final states

Final States	Requirements in each of 3 consecutive trigger banks	Requirement in Calorimeter
≥1μ	$A \cdot \bar{B}^a$	none
≥2μ	≥2 in A or B	≥20 GeV deposited ≥2 modules upstream
≥3μ	≥3 in A or B	none

[a] "B" refers to S_3-S_{10} in Figs. 1 and 2; "A" refers to S_1, S_2, S_{11}, and S_{12}.

shown in Fig. 3. Although spread over many cathode strips, the induced charge produces a count only in the one or two electronics channels closest to the peak, even when the pulse height far exceeds threshold. Through a specially stabilized amplifier, each calorimeter scintillator feeds two ADC's, which together operate over a range of 0.03 to 1500 equivalent minimum-ionizing particles. The resolution on hadron energy E_{had}, calibrated using inelastic muon scattering, is $1.5E_{had}^{1/2}$ (GeV).

The spectrometer was triggered in parallel by ≥1, ≥2, or ≥3 muons in the final state. The required signatures in the scintillator hodoscopes and calorimeter counters are listed in Table 1. The multimuon triggers could not be vetoed by hodoscope and calorimeter information; the ≥1μ and ≥3μ triggers were affected in no way by the calorimeter signals. Under some conditions, when more than one count was required from a scintillator hodoscope, two of the contributing hodoscope elements were required not to be adjacent. During the run the instantaneous beam intensity varied from 0.03 to 0.11 muon per RF bucket. Each bucket was separated from the next by 19 nsec. The trigger was vetoed by halo muons in the same RF bucket, or beam muons in the same or adjacent buckets. The deadtime thereby induced ranged up to ∿50%. As many as ∿60 events/1-sec spill were recorded on a PDP-15 computer with read-in deadtime ≲15%.

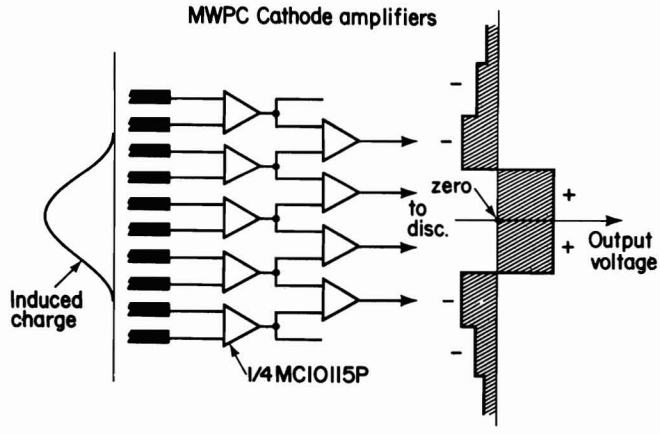

FIG. 3. Network of differential amplifiers sensing the center of the charge distribution induced on proportional-chamber cathode strips. The outputs feed conventional MWPC discriminators. If the cathode-strip spacing is ∿ half the plane spacing, one or two channels register with ∿ equal probability, providing a vernier position measurement.

Beam muons were momentum-analyzed by systems of proportional chambers and scintillator hodoscopes interspersed between magnets producing two separate beam deflections. Pulse heights from calorimeter counters within the spectrometer provided a tentative longitudinal vertex position. The beam track then was traced forward to this vertex using the PC and DC hits. Outgoing tracks were recognized initially at their downstream end. Hits were added extending the tracks upstream to the vertex, making adequate allowance for Coulomb scattering and momentum uncertainty. In order not to interfere with rejection of halo tracks or later use of outgoing tracks to pinpoint the vertex, the transverse vertex position was not allowed to influence this upstream projection. At least 4 PC hits in two views and 3 hits in the third view were required for each accepted track. The small electromagnetic showers found along high energy muon tracks in iron, due mainly to direct production of electron pairs, contributed extra hits in the wire chambers which were not completely rejected at this stage. After the full track was identified, it was possible to apply a momentum-fitting algorithm capable of solving for the Coulomb-scattering angle in each magnet module, yielding a rigorous χ^2 for the track. By iteration, this algorithm identified and suppressed the false extra hits.

The beam and secondary tracks next were examined for consistency with a common vertex. The vertex position was moved by iteration in 3 dimensions to minimize the overall χ^2 while including all associated tracks. After the vertex was fixed, the coordinates and momentum of each track were redetermined, subject to the condition that it intersect the vertex point.

For analysis of some 1μ final states (inelastic scattering) and some 3μ final states (ψ production), the events were subjected to a 1-constraint fit demanding equality between the beam energy at the interaction point and the sum of muon and hadron shower energies in the final state. Using error matrices produced by the fits to individual tracks, the constraint perturbed all components of each track momentum. The resulting momentum resolution is 7%-12% (typically 8%) per track. At the ψ mass, the dimuon mass resolution is 9%. The uncertainty in Q^2 typically is 10%, but is bounded below by $\sim$0.15 $(\mathrm{GeV/c})^2$ because of track angle uncertainty.

The acceptance and resolution of the spectrometer were modeled by a complete Monte Carlo simulation. Coordinates of randomly sampled beam muons were used to represent the beam. Simulated muons underwent single and multiple Coulomb scattering, bremsstrahlung, and other energy-loss straggling in the steel magnet plates. Their trajectories were deflected in each plate by the precisely mapped magnetic field. Simulated interactions occurred between muons and nucleons in non-degenerate Fermi motion, or coherently between muons and Fe nuclei. At low momentum transfer the effects of nuclear shadowing were taken into account. Coherent and elastic processes were attenuated by the appropriate form-factors even for forward scattering (at $|t|_{min}$). Detector resolutions and efficiencies were included throughout. Monte Carlo events were output in the same magnetic tape format as raw data, and were reconstructed, momentum-fit and histogrammed by the same programs.

Data were accumulated during the first half of 1978 using $\sim 4\times10^{11}$ (gated) 209 GeV muons, of which $\sim$90% were μ^+. Approximately 5×10^9 90 GeV μ^+ also were used. The extent of the data is shown in Table 2. Events with 2 or 3 muons in the final state, or with $Q^2>50$ $(\mathrm{GeV/c})^2$, are not rare in this experiment -- at least 10^5 of each category are on tape. Results presented here are based on 20% of this sample.

Table 2. Extent of data.

Final State	Cuts	Total on Tape
1μ	$Q^2>10$	10^6
	$Q^2>50$	10^5
	$Q^2>100$	10^4
2μ	$E_{slow} \gtrsim 10$ GeV	2×10^5
3μ	$E_{slow} \gtrsim 10$ GeV	2×10^5
	ψ (background subtracted)	10^4

One-Muon Final State

The acceptance for muon scattering at 209 GeV is exhibited in Fig. 4. The maximum acceptance is not unity because of the trigger requirement of a near-vertical scatter, which largely decouples the measurement of scattered energy and angle. The acceptance drops off above $\theta \gtrsim 0.2$ due to magnet size, and more gently at low Q^2 as the acceptance cuts off for downstream segments of the target. This gentle cutoff ensures sufficient low-Q^2 acceptance without excessive data rate. At E = 90 GeV the acceptance vs. $Q^2/2ME$ and $(E-\nu)$ is nearly the same, reducing the minimum accepted Q^2 by the ratio of beam energies.

At the time of this conference the single-muon analysis already offers a number of strong features. The Fermilab beam intensity permits redundant momentum tagging of each beam muon. Within ±28 (±9) nsec, extra beam (halo) muons are removed from analysis by the trigger veto. Both the incident and scattered tracks are constrained to a common vertex typically localized within $0.1\times0.2\times10$ cm^3. Scattered tracks are constrained typically by $\sim$30 separate transverse coordinate measure-

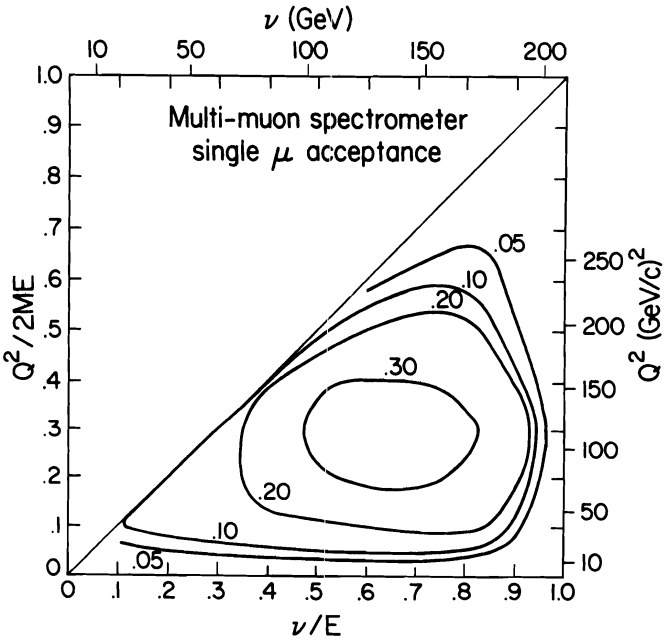

FIG. 4. Calculated detection efficiency vs. Q^2 and ν for inelastic scattering of 209-GeV muons. An average over the full target length is shown. If the target is restricted to the few modules furthest upstream, the acceptance at low Q^2 is much more uniform.

ments. Over 80% of raw triggers survive final cuts. Nevertheless, the analysis is not yet mature. Improvements now being tested will optimize the use of drift chambers and the localization of vertices. Calibration of incident and scattered energies is being tightened from ∿1% to ∿0.2%. Underway are efforts to simulate more fully the effects of shower-induced extra hits and stale tracks, and to iterate the Monte Carlo guess-function (currently the Chicago-Harvard-Illinois-Oxford fit[4]). The effects of these improvements cannot be fully anticipated. In Figs. 5-8 we have chosen to exhibit statistical errors only, discussing in text the likely stability of individual features.

In lieu of separating the structure functions we quote $F_2(x,Q^2)$ [neutron + proton average, corrected for Fermi motion] assuming the longitudinal/transverse photon cross-section ratio

$$\sigma_L/\sigma_T = (1.6 - 0.7x)\, Q^2/(1.1 + Q^2)^2.$$

This choice has the correct low-Q^2 asymptote, fits the SLAC-MIT data[5] very well, and is consistent at high Q^2 with the CERN-Dortmund-Heidelberg-Saclay (CDHS) null result[6]. Other measurements of F_2 used for comparison to these data have been adjusted to this same σ_L/σ_T[7].

In the Buras-Gaemers QCD parameterization[8] of scale-noninvariance in $F_2(x,Q^2)$, the slope $\partial \ell n F_2/\partial s$ [$s \equiv \ell n\,(\ell n\, Q^2/\Lambda^2)$] depends on Q^2 only to the extent that F_2 significantly changes its x-dependence within the Q^2 range. Because such changes are modest, $\ell n F_2$ is expected to vary nearly linearly with s. Numerical computation confirms this expectation[9]. The first-order effect of varying Λ is merely to adjust the scale of s. Rudimentary comparison of various data sets with QCD expectations is facilitated by fixing Λ at some reasonable value (we fix Λ=0.3 in the definition of s) and plotting $\ell n F_2$ vs. s. The slopes $\partial \ell n F_2/\partial s$ are determined by straight-line fits to these plots and displayed vs. x. Comparison with the predictions of Buras and Gaemers for $\partial \ell n F_2/\partial s$ directs attention to the issue of scale-noninvariance, rather than to small differences in the parameterization of the x-dependence of F_2 at fixed Q^2.

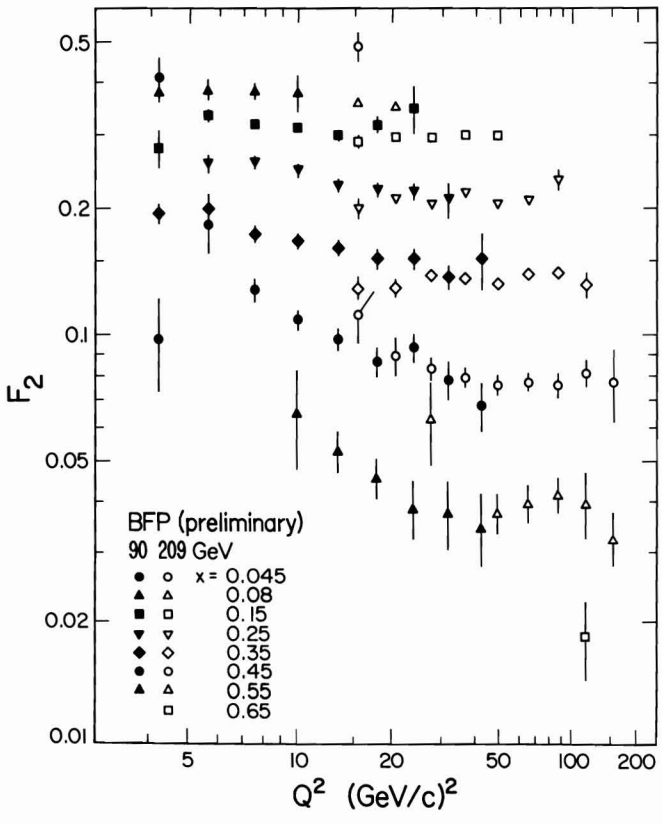

FIG. 5. $F_2(x, Q^2)$, average for neutron and proton, measured in scattering of 209-GeV and 90-GeV muons from an iron target with nuclear effects removed. The value $\sigma_L/\sigma_T=(1.6-0.7x)Q^2/(1.1+Q^2)^2$ is assumed. F_2 is measured at the x values indicated, *not* at the average x of data within a bin. The abscissa is linear in $\ell n(\ell n(Q^2/0.09))$. Only statistical errors are indicated.

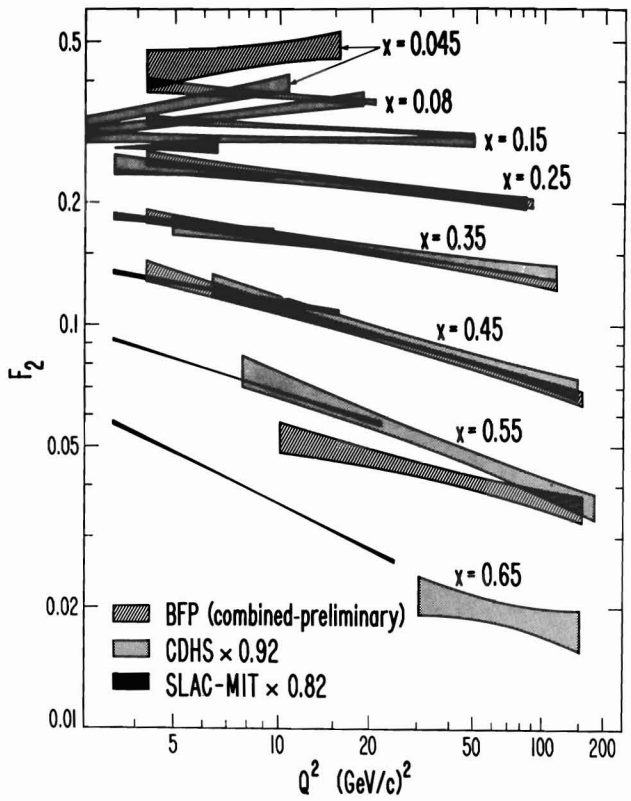

FIG. 6. One-statistical-standard-deviation limits obtained from fits to structure-function data from BFP (this experiment), CDHS (Ref. 6),and SLAC-MIT (Ref. 13). The fits are linear in $\ell n(F_2)$ vs. $\ell n(\ell n(Q^2/0.09))$. All data are referenced to the same σ_L/σ_T as in Fig. 5. The indicated normalization factors are applied only to clarify the comparison; there is no implication that these factors produce the correct absolute normalization for the SLAC and CDHS samples. Other small adjustments have been made to CDHS data (see text).

Figure 5 exhibits the BFP data plotted according to this prescription. The 209-GeV (open) points, with $15 \le Q^2 \le 150$, are compressed into the right-hand half of the figure (Δs=0.37). The NA-2 iron target data[10] (Δs=0.42) and the NA-4 data[11] (Δs=0.31) reported to this conference would appear similarly compressed on such a plot. Completion of the picture requires addition of the BFP 90-GeV data (solid points), giving a total range in s similar to that of CDHS[6]. Taken alone, the open points show little scale-noninvariance. However, because their range in s is small, little variation is expected. For example, for x=0.35 and Λ=0.4, the Buras-Gaemers fit[8] gives only a ±8% "tilt" over the six central high-statistics 209-GeV points at that x. Our best current estimate of systematic error in

that region is obtained from the comparison of F_2 measured at the same x and Q^2, but different beam energy (hence different θ and E'). If the parameterization of σ_L/σ_T is nearly right, the occasional $\sim$10% differences revealed in that comparison must be interpreted as manifestations of systematic error. We conclude that the data do not yet reliably discern *changes* in $\partial \ell n F_2/\partial s$ over the measured range. Only the *average* slope over the full range in s is prudently fitted[12].

Figure 6 displays the $\pm 1\sigma$ limits of such fits to BFP, CDHS[6], and SLAC-MIT[13] data. The CDHS points have been multiplied by $5(1-0.01(1-x)^3/x^{\frac{1}{2}})/18$, where the x-dependent term is a quark sea correction. A Fermi motion correction no larger than +5% (at x=0.45) has also been applied to these points. In addition, the values of F_2 quoted by CDHS refer not to the center of the x bin, but to the average x of whatever data fell within the bin[14]. Assuming (crudely) that the x distribution of data within the bin is that of F_2, we have applied a further correction to the CDHS points which is as large as -9% at x=0.65. The linear parameterization of $\ell n F_2$ vs. s generally affords a good fit to the CDHS and SLAC-MIT data[15]. The three data sets are in fair agreement, except that CDHS and BFP are normalized 10±2% and 18±2% below SLAC-MIT in the region of their overlap. The BFP scale error, currently quoted at 14%, should shrink as the absolute normalization receives further scrutiny.

The x-dependence of F_2 is best determined at $Q^2(x)$ where BFP data exist at both energies. With the choice $Q^2 = 50x^{\frac{1}{2}}$, the x-dependence of F_2 is exhibited in Fig. 7 for BFP and CDHS. The muon data appear to vary more steeply with x than do the neutrino data. The most significant difference is at $x > 0.5$, where

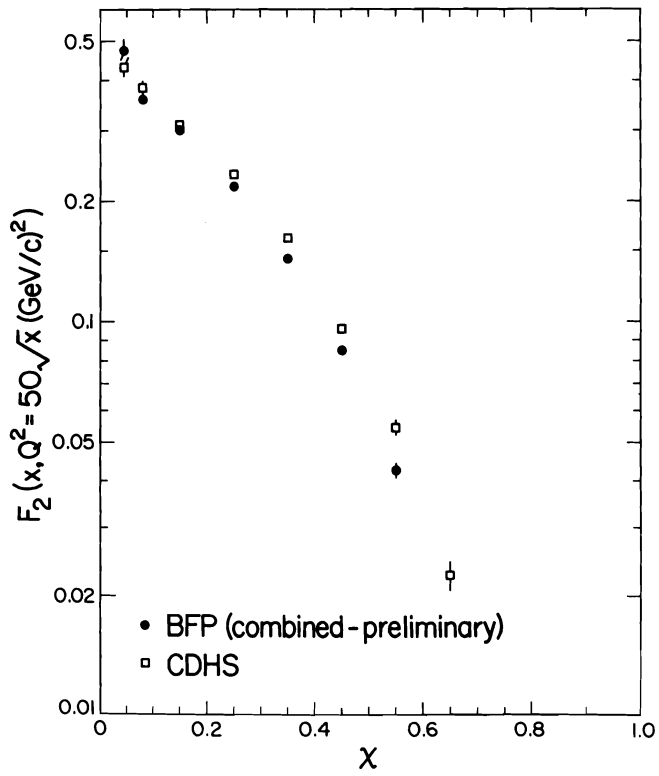

FIG. 7. $F_2(x, Q^2=50\sqrt{x})$ obtained from fits shown in Fig. 6 to data from BFP (this experiment) and CDHS (Ref. 6). The CDHS data plotted here do *not* contain the normalization factor 0.92 used in Fig. 6.

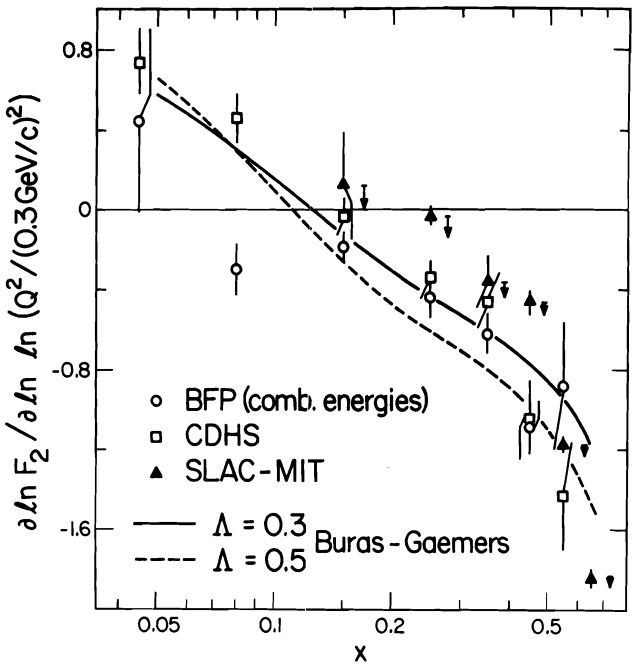

FIG. 8. Scale-noninvariant slopes $\partial \ell n F_2/\partial \ell n(\ell n(Q^2/0.09))$ obtained from fits shown in Fig. 6 to data from BFP (this experiment), CDHS (Ref. 6), and SLAC-MIT (Ref. 13). The slopes are compared to predictions from the fit of Buras-Gaemers (Ref. 8) to earlier data. The value Λ=0.3 GeV was their best fit; the curve with Λ=0.5 GeV indicates the sensitivity to Λ. The downward-pointing arrows adjacent to SLAC-MIT points show the small changes in slope predicted by the Buras-Gaemers fit as Q^2 varies from the SLAC-MIT range to the CDHS/BFP range. Only statistical errors are indicated; systematic errors associated with energy calibration are dominant in BFP data below x=0.1.

the sensitivity of analyses to resolution parameterization and method used to extract F_2 is most severe.

The crucial issue of scale-noninvariance is addressed in Fig. 8. The extent to which the fitted slopes $\partial \ell n F_2/\partial s$ indeed are expected to remain Q^2-invariant is revealed by the downward-pointing arrows. These indicate the very small changes in slope predicted by the Buras-Gaemers fit (Λ=0.3) as Q^2 increases from the SLAC-MIT to the BFP/CDHS range. Were it not for target-mass corrections probably important in the SLAC Q^2 range, the three sets of data would be directly comparable. In any event, the SLAC-MIT slopes vary more steeply with x than do the BFP, CDHS, or Buras-Gaemers slopes. In particular, the SLAC-MIT slope at x=0.25 is uniquely close to zero, as also indicated by Mestayer[16]. Another apparent anomaly is the negative $\partial \ell n F_2/\partial s$ fitted to BFP data at x=0.08. Since the sensitivity of F_2 to calibration of reconstructed muon energies is found to be critical below x=0.1, we regard that region as not yet reliably measured by BFP data.

Above x=0.2, the BFP and CDHS data independently show clear evidence for scale-noninvariance over the full Q^2 range. The values of $\partial \ell n F_2/\partial s$ measured by the two experiments are in excellent agreement with each other, and with the fits of Buras and Gaemers if $\Lambda \sim 0.3$ to 0.5 GeV. Remarkably, for $x > 0.2$ the Buras-Gaemers slopes agree better with those of BFP and CDHS than with the earlier data upon which their fits were based.

Three-Muon Final State

Analysis of 3μ final states so far has focussed on the virtual photoproduction of J/ψ(3100). In July 1979 the BFP group published[17] the first measurement of this process. Subtleties in the analysis associated with muon pairing, mass-continuum subtraction, correction for nuclear effects, and extrapolation to t=0 are discussed fully in Refs. 17 and 18. Figure 9, taken from Ref. 17, shows the agreement between the forward elastic ψ-production cross-section as determined from photoproduction[19-22] and from muoproduction using the equivalent-photon approximation. A QCD calculation[23] using the "photon-gluon fusion" diagram (hatched band) predicts a steeper energy-dependence than is observed above E_γ=30. Within vector-meson dominance (VMD), the ratio of the solid line to the broken line ($p^{\psi}_{c.m.}{}^2/p^{\gamma}_{c.m.}{}^2$) gives the energy-dependence of the square of the ψ-nucleon total cross section.

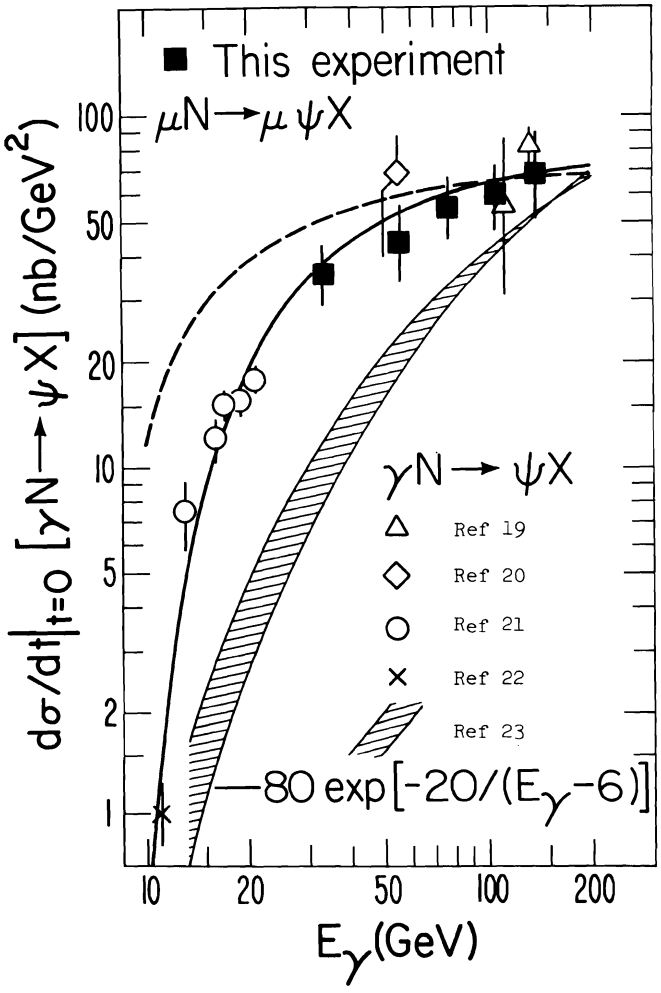

FIG. 9. Energy-dependence of ψ photoproduction at t=0. The muoproduction points (squares) use an equivalent-photon approximation. Not indicated is their ±30% normalization error. The dashed curve is a VMD threshold factor (see text), and the hatched band is a QCD calculation. Both the QCD prediction and the muoproduction points in fact represent cross-sections integrated over t and divided by a t slope of 2.4 (GeV/c)$^{-2}$ (details are in Refs. 17 and 18).

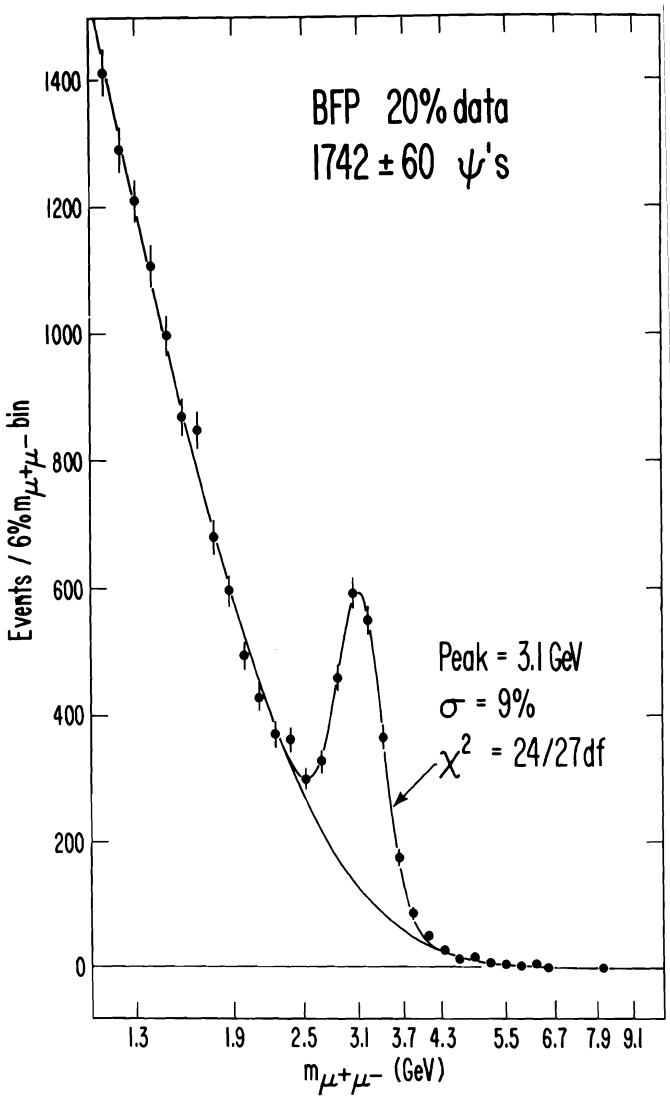

FIG. 10. Invariant-mass spectrum of muoproduced $\mu^+\mu^-$. The curve is a fit to
$dN/dm_{\mu\mu} = g(u)\exp(f(u)) + h\exp(-u^2/(2(.09)^2))$
where $u=\ell n(m_{\mu\mu}/3.1)$, f and g are quadratic and cubic polynomials in u, and $\exp(f(u))$ is a best fit to the continuum outside the ψ region.

The 20% of BFP data presently analyzed yield 1742±60 fully-reconstructed muoproduced ψ's, more than 80% of the world sample[10,11]. The dimuon invariant-mass spectrum is exhibited in Fig. 10. The total cross section including cascade decays to the ψ, corrected for nuclear effects, is

$$\sigma(\mu N \to \mu\psi X) = 0.67 \pm 0.20 \text{ nb}$$

at 209 GeV, where the error is dominated by normalization uncertainty. About 1/3 of the events leave a significant [>(7±3) GeV] energy deposit in the calorimeter. This energy comes from hadrons produced at the hadron vertex, decay products of particles cascading into the ψ, and radiative corrections. Since we are still working to separate these contributions, differential results are available only for events consistent in the calorimeter with elastic ψ production.

In the elucidation of mechanisms for hadronic production of the ψ, study of the polar angular distribution of its decay products has been particularly

fruitful. The same has been true for electroproduction of the light vector mesons. Under the assumption of natural-parity exchange and s-channel helicity conservation, the relative production rate for longitudinally and transversely polarized vector mesons is the product of the photon polarization flux ratio $\varepsilon = \Gamma_L/\Gamma_T$ and the cross-section ratio $R_V = \sigma_L/\sigma_T$, where V denotes vector meson. At lower energies, both R_ρ[24] and R_ϕ[25] are measured to be consistent with $R_V = 0.5\ Q^2/m_V^2$, where m_V is the vector-meson mass. Somewhat smaller R_ρ is observed at Fermilab energies[26]. The precision of these experiments is not sufficient to rule out the possibility that R_V is independent of m_V.

Averaged over azimuth, the angular distribution of either muon in the decay of muoproduced ψ's is, with the aforementioned assumptions[27],

$$W(\cos\theta) = \frac{1}{1+\varepsilon R_\psi}\frac{3}{8}\ \{1+\cos^2\theta + 2\varepsilon R_\psi \sin^2\theta\},$$

where θ is the polar angle in the Gottfried-Jackson frame. For BFP data, ε=0.81 essentially independent of Q^2. In a fit to $W=W_0(1+\eta\cos^2\theta)$, the coefficient of $\cos^2\theta$ is

$$\eta = (1-2\varepsilon R_\psi)/(1+2\varepsilon R_\psi).$$

Figure 11(a) shows that the angular distribution for data integrated over Q^2 is consistent with fully transverse ψ polarization. By itself this result may discriminate between VMD and "photon-gluon fusion" approaches[23,28,29] to the description of ψ photoproduction. The latter process, described by a Bethe-Heitler graph with e^+e^- replaced by $c\bar{c}$ and the nuclear photon replaced by a gluon, must include the exchange of a second gluon so that the $c\bar{c}$ pair can remain a color singlet. If this vector exchange can be expected to depolarize the ψ[30], the "photon-gluon fusion" model fails.

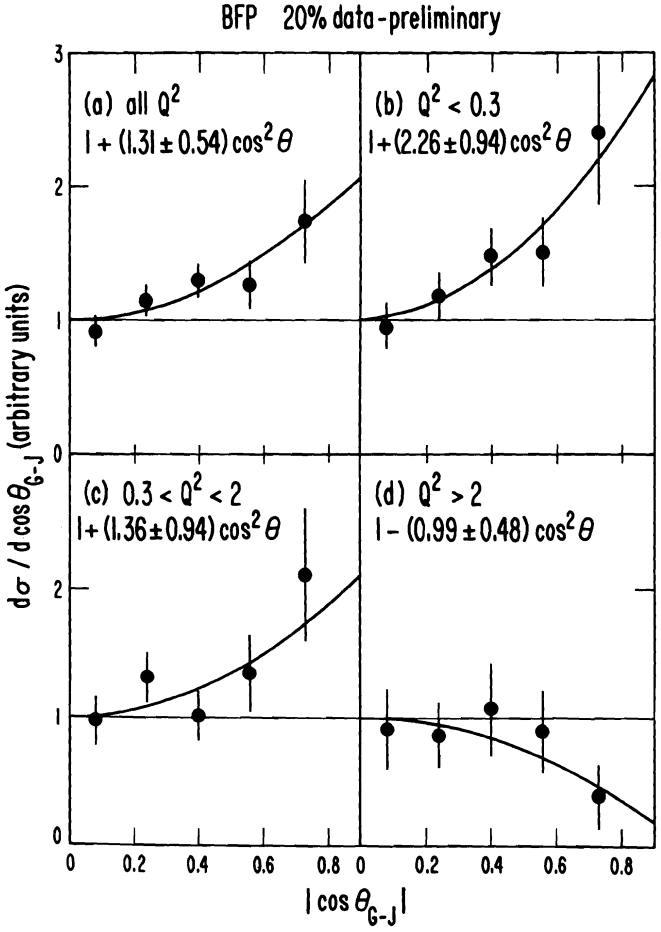

FIG. 11. Polar angular distribution of ψ-decay muons in the Gottfried-Jackson frame, folded about 90°: (a) all data; (b)-(d) data divided into three Q^2 regions. The curves and the coefficients of $\cos^2\theta$ are the fits to $W(\cos\theta)$ described in the text.

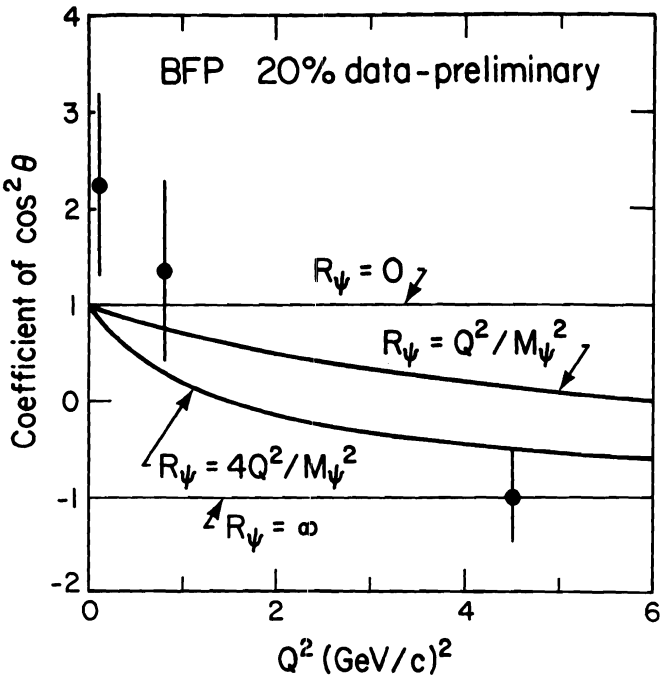

FIG. 12. Coefficients of $\cos^2(\theta)$ from fits displayed in Fig. 11, plotted vs. Q^2 for each region. Indicated are expectations for transverse, longitudinal, and intermediate ψ polarization with two Q^2-dependences. The lower curve is the best fit. A VMD extrapolation from light-vector-meson electroproduction lies between the upper curve and R_ψ=0.

Figure 11(b)-(d) exhibits the behavior of the coefficient of $\cos^2\theta$ as Q^2 increases. As for all other distributions, each data point is the result of an individual subtraction of the muon-pair mass continuum. Our preliminary conclusion is that the coefficient of $\cos^2\theta$ does not remain invariant as Q^2 rises. Rather, there is indication of a transition from predominantly transverse to predominantly longitudinal polarization. Figure 12 displays the coefficient of $\cos^2\theta$ vs. Q^2. The fit to $R_\psi = \xi_\psi{}^2 Q^2/m_\psi^2$ yields $\xi_\psi{}^2 = 4.0\ ^{+5.4}_{-2.1}$ (11% confidence), 2.6 standard deviations above the VMD extrapolation from lower-energy ρ and ϕ data, $\xi^2_{\rho,\phi} \cong 0.5$. The ψ data would become quite consistent with ρ and ϕ results if the growth of σ_L/σ_T were imagined to be *independent* of the scale set by the vector-meson mass.

A goal of the ψ analysis is determination of the Q^2-dependence of the ψ-virtual photon coupling strength. If the VMD coupling $\gamma_\psi{}^2/4\pi$ is fixed, the only Q^2-dependence remaining in that model is that of the ψ propagator $(1+Q^2/m_\psi{}^2)^{-2}$. Figure 13 depicts the current best fit to this parameterization, with mass parameter

$$\Lambda = 2.7 \pm 0.3\ \text{GeV}.$$

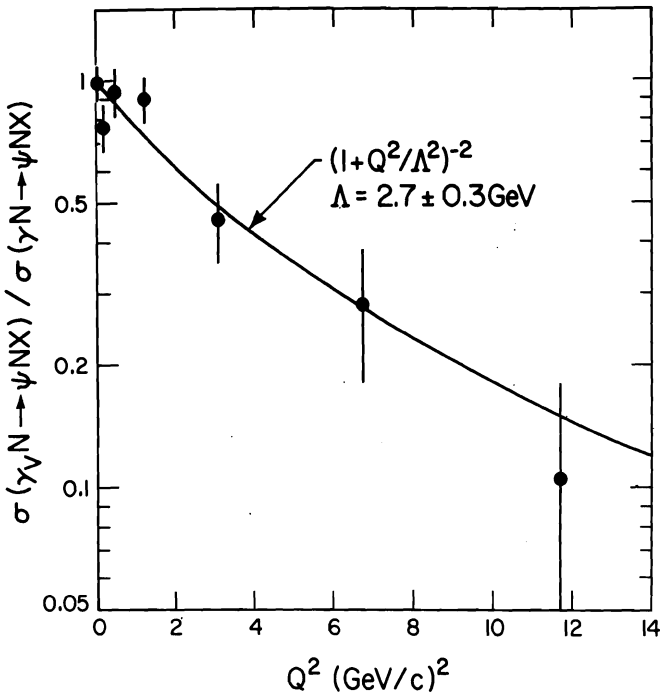

FIG. 13. Q^2-dependence of ψ production by the equivalent-photon flux, neglecting its longitudinally polarized component. The small attenuation at high Q^2 due to $|t|_{min}$ effects has been removed. Without this correction, the ordinate would be very nearly equal to $Q^2 d\sigma/dQ^2$ for ψ muoproduction. The data are normalized to unity at the lowest-Q^2 point (Q^2=0.06). Indicated is a best-fit propagator consistent with ψ dominance; however, the true propagator mass could be ∿2× smaller if σ_L/σ_T rises with Q^2 as rapidly as is suggested by Fig. 12.

The apparent strong Q^2-dependence of R_ψ has a major effect upon the interpretation of this result. For example, dividing through by $(1+\varepsilon f \xi^2 Q^2/m_\psi{}^2)$, where f is the ratio of detection efficiencies for longitudinal and transverse $\psi \to \mu^+\mu^-$ decay, should isolate the Q^2-dependence of the ψ coupling to transverse photons. Using our central value for ξ^2, the fit to this quotient produces a Λ which is smaller by a factor of ∿2 than the value quoted above! Evidently, the description of ψ muoproduction by VMD with fixed $\gamma_\psi{}^2/4\pi$ agrees with the data only in a restricted sense. The restriction is the necessity for assuming that σ_L/σ_T in fact is much smaller than the preliminary data indicate.

Two-Muon Final State

The remainder of this report is devoted to exploratory areas in which comparison to other muon data presently is not possible. For 2μ final states our quantitative emphasis is on extraction of structure functions for muoproduction of open charm. Still in progress, this analysis requires precise subtraction of contamination from π and K decays, and careful choice of a $c\bar{c}$ production model for use in simulating apparatus acceptance. Available for this conference are the results of a search for "extra" muons possessing unusual kinematics which might reveal new production processes. A kinematic variable of obvious interest is $p_\perp$, the muon momentum transverse to the virtual photon direction. Processes such as weak production of a new heavy lepton, or (by extrapolation of our ψ results) muoproduction of $b\bar{b}$, would associate high $p_\perp$ with higher-than-usual Q^2 at the lepton vertex.

Figure 14 exhibits the $p_\perp$ spectrum in three Q^2 bands for (a) opposite-sign and (b) same-sign extra muons. Events in this sample satisfy the 2μ trigger and contain exactly two reconstructed final-state muons (the scattered muon is taken as the more energetic). Though uncorrected for acceptance, all six spectra give acceptable fits in the region $0.8 < p_\perp < 1.8$ GeV/c to $dN/dp_\perp \propto \exp(-Bp_\perp)$, with B=3.3. When the fits are extrapolated above $p_\perp$=1.8, all but the same-sign data at $Q^2 > 9$ (GeV/c)^2 show no indication of an excess above the extrapolation.

The few events contributing to the excess in the latter category are best examined in Figs. 15(a) and (b), which exhibit the two-dimensional distribution of events vs. $p_\perp$ and $\sqrt{Q^2}$. The opposite-sign data in Fig. 15(a) contribute up to ∿1000 events/bin at low $p_\perp$ and low Q^2, but no events to the high-$p_\perp$, high-Q^2 region outside the empirically-drawn heavy line[31]. The six same-sign events outside the heavy line in Fig. 15(b) have $\langle p_\perp \rangle \sim 3$ GeV/c and $\langle Q^2 \rangle \sim 25$ (GeV/c)^2. Physicists have checked the reconstruction of each of these events by hand, using the procedures discussed in the next section. In two events there are indications of a third muon track too soft ($\lesssim 5$ GeV) to reconstruct. The events are equally divided between positive ($\mu^+\mu^+$ final state) and negative ($\mu^-\mu^-$ final state) beam polarity. Their typical ν (∿150 GeV) is ∿1.5× the full-sample average, and the typical daughter energy (∿40 GeV) is twice that average. Thus, the final state muon energies are sufficiently symmetric to satisfy an analogue of the Pais-Treiman test[32]. The missing-energy distributions in Fig. 16 reveal no additional difference between these six events and the full 35 539-event sample[33].

An example of a process capable of producing high-$p_\perp$ "extra" muons at high apparent Q^2 is the weak production and μμν decay of heavy leptons M^0 and M^{++}. For example, 60% of the events arising from simulated production and decay of a 9-GeV M^{++} populate the high-$p_\perp$ high-Q^2 side of the heavy line in Fig. 15(b). Comparison of simulated and observed populations in this region gives rise to the mass-dependent limits plotted in Fig. 17 for M^{++} and M^0 production by 209-GeV μ^+. The incident muon is assumed to be coupled to the M by means of a right-handed weak current. The dashed line exhibits the level expected if the current has Fermi strength and if the $M \to \mu\mu\nu$ branching ratio is 0.1. In the absence of a special mechanism to suppress pair-production, doubly-charged leptons in this mass range would have been seen at PETRA. No comparable limits on M^0 production are available from any other experiment. One early argument for existence of the M^0, the "hybrid" gauge model, is disfavored by the SLAC-Yale measurements[34] of helicity asymmetry in electron scattering.

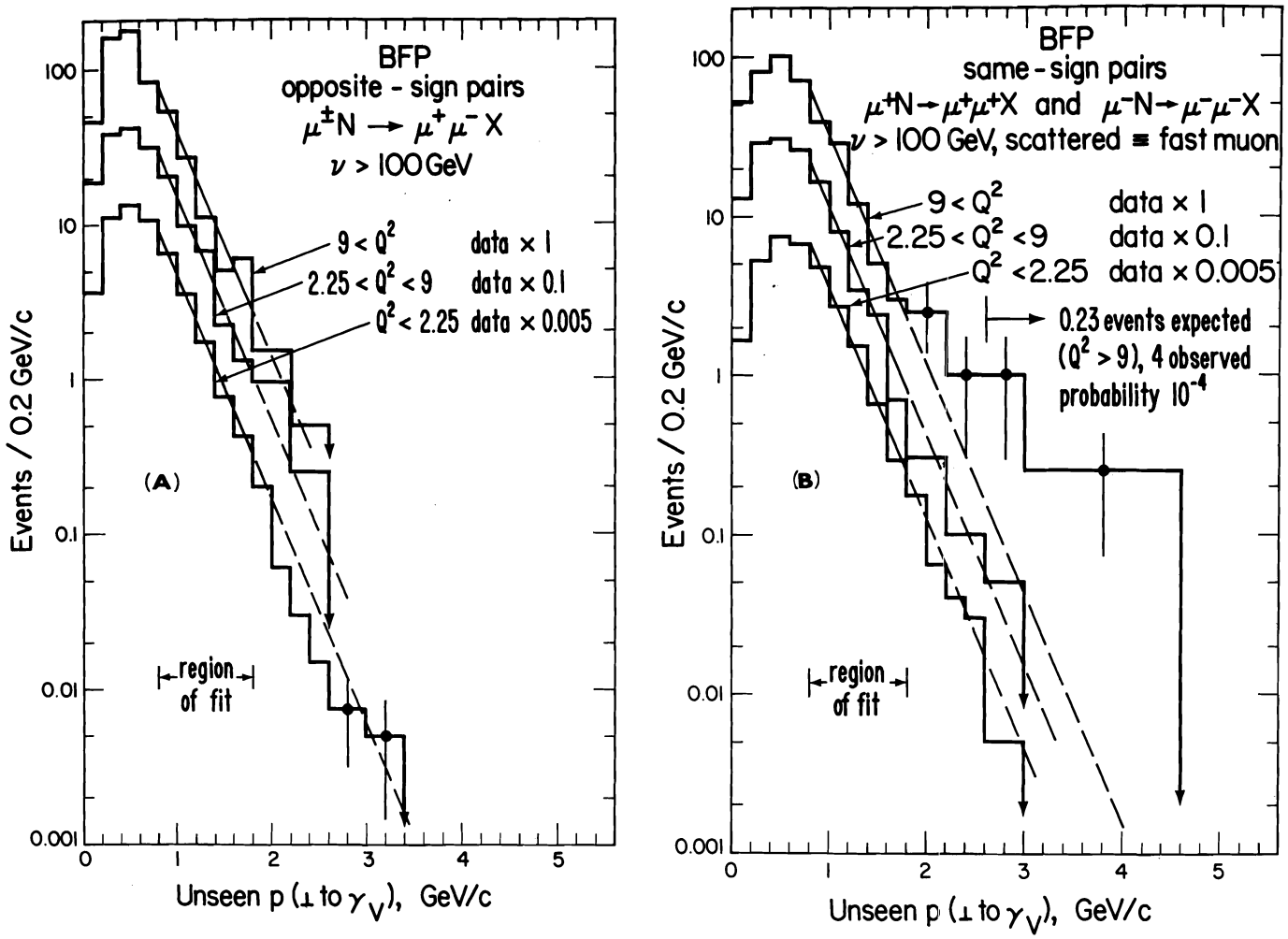

FIG. 14. Spectra of momenta transverse to the virtual-photon direction for singly produced "extra" muons having (a) opposite and (b) same charge as the scattered muon. Data are divided into three Q^2 bands and are not acceptance-corrected. Solid lines show an acceptable simultaneous fit to all six spectra in the region $0.8 < p_\perp < 1.8$ GeV/c. Dashed lines extrapolate this fit to high $p_\perp$. A statistically significant excess over this extrapolation is seen at high $p_\perp$ and high Q^2 in the same-sign data.

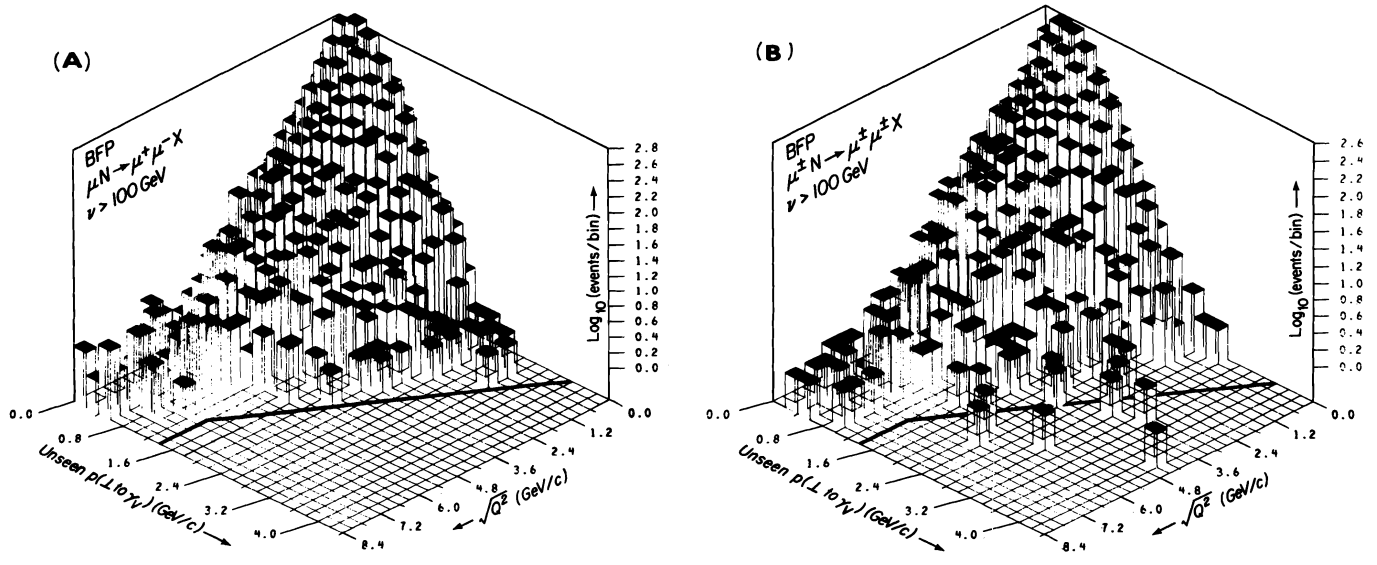

FIG. 15. Two-dimensional distribution of singly-produced (a) opposite-sign and (b) same-sign muons displayed vs. $\sqrt{Q^2}$ and muon momentum transverse to the virtual-photon direction. Since the vertical scales are logarithmic, the bin populations range from ∿1000 to 0. The empirically-drawn solid line (Ref. 31) contains all data except for six same-sign events with $\langle p_\perp \rangle \approx 3$ GeV/c and $\langle Q^2 \rangle \approx 25$ (GeV/c)^2.

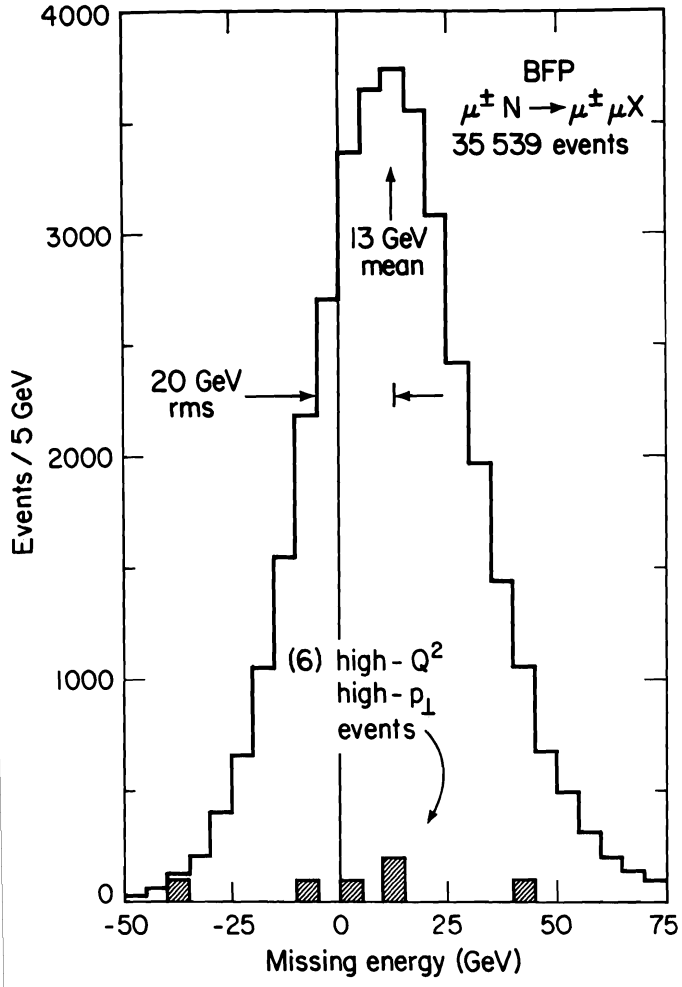

FIG. 16. Difference between incident muon energy and sum of final-state muon and hadron energies, for data with a singly produced "extra" muon. The six high-Q^2 high-$p_\perp$ events in Fig. 15(b) are typical of the full sample in this variable.

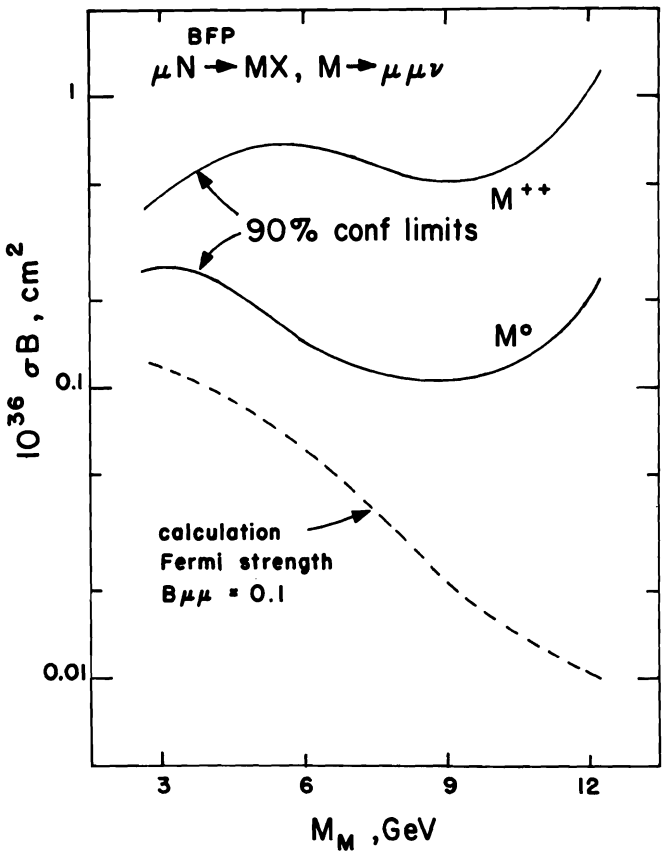

FIG. 17. 90%-confidence limits on production by 209-GeV μ^+ of neutral and doubly-charged heavy leptons of mass M_M decaying to $\mu\mu\nu$. If the beam muon were coupled to such leptons by a right-handed weak current of Fermi strength and if the $\mu\mu\nu$ branching ratio were 0.1, the signal level would be that indicated by the dashed line.

Five- and Four-Muon Final States

We define "rare" events as those having ≥ 4 muons or 2 missing leptons in the final state. Identification of rare events begins in the programs which reconstruct muon tracks and fit their momenta. Events satisfying normal analysis criteria which possess unusual characteristics are saved on microfilm containing tabulated data and computer-generated track pictures. A double scan by physicists of the microfilm identifies a small sample of candidates for which are generated $\sim$1 m^2 pictures containing all raw wire chamber hits, resolved to better than 1 mm in real transverse coordinates. With the high-resolution pictures, raw chamber hits are reconstructed by hand into tracks and the vertex position determined. The track reconstruction program then is forced to fit the event using the hand-selected information. To be accepted as a rare event, the result of this hand-forced fit is required to differ in no significant respect from that of the original reconstruction. Close inspection of each high-resolution picture insures that additional tracks crossing as few as 3 chambers have not been missed, and that distinct tracks separated along their full length by as little as 5 mm have not been combined.

A particular concern, that two interactions not mistakenly be superimposed, is satisfied by four precautions: (1) The trigger demands only one beam track within a 57-nsec window centered on the event. (2) All tracks are required to emanate from a tightly defined common vertex. (3) All tracks are required to intersect the appropriate fine-grained hodoscope scintillators, sensitive within a ±10-nsec window. (4) Adjacent drift and proportional chamber hits are required to register at a level rejecting tracks out of time by more than $\sim$50 nsec. The accepted tracks satisfy a tight χ^2 cut separately in both orthogonal views. At least three hits in the third view unambiguously link the two projections. Each accepted track, passing smoothly through >12 absorption lengths of steel, can be interpreted only as a muon. The sign of each muon's charge is at least 8 standard deviations from the reversed value.

Table 3 presents the properties of four rare events found in an initial scan of 20% of the data. They consist of one 3μ event with two missing μ^- or ν_μ, one 4μ event with large pair masses, and two 5μ events. The efficiency of the initial scan exceeded 50%, with the possible exception of the 3μ event type. Although model-dependent, the detection efficiencies

TABLE 3. Properties of rare events.

Event	Scattered Muon	Energies (GeV)	Masses (GeV/c^2)	Unseen $p_\perp$ to $\gamma\gamma$ (GeV/c)
851-5726	2	E_3= 19± 2	M_{34}=0.5±0.1	0.3±0.1
$\mu^-\to\mu^-\mu^+\mu^+$	Q^2=0.1±0.1	E_4= 11± 2		
1 2 3 4	ν =160±6	E_{had}=103±15		
		E_{miss}= 27±17		
1191-5809	2	E_3= 26± 3	M_{34}=3.0±0.3	2.0±0.2
$\mu^+\to\mu^+\mu^+\mu^-\mu^-$	Q^2=0.3±0.2	E_4= 18± 2	M_{35}=3.2±0.3	
1 2 3 4 5	ν =158±7	E_5= 25± 4	M_{345}=4.6±0.3	
		E_{had}> 57±11		
		E_{miss}< 31±14		
1208-3386	2	E_3= 50± 5	M_{35}=1.3±0.2	0.1±0.3
$\mu^+\to\mu^+\mu^-\mu^-\mu^+\mu^+$	Q^2=0.2±0.2	E_4= 27± 3	M_{36}=0.3±0.1	
1 2 3 4 5 6	ν =149±9	E_5= 61± 6	M_{45}=0.4±0.1	
		E_6= 10± 2	M_{46}=0.5±0.1	
		E_{had}= 6± 3	M_{3456}=2.0±0.2	
		E_{miss}= -4±13		
851-11418	Q^2=3.5±0.6	E_3= 13± 2	M_{34}=2.3±0.2	1.8±0.4
$\mu^-\to\mu^-\mu^-\mu^+\mu^+\mu^-$	ν = 61±12	E_4= 19± 2	M_{35}=2.0±0.2	
1 2 3 4 5 6		E_5= 15± 2	M_{46}=0.5±0.1	
		E_6= 10± 2	M_{56}=0.3±0.1	
		E_{had}= 5± 3	M_{3456}=3.5±0.3	
		E_{miss}= -1±13		

for these events may be estimated to lie typically in the 10-20% range. Each event therefore represents a cross section of order 3×10^{-38} cm^2/nucleon.

Three-muon event (two missing leptons)

Four events of this type have been produced by neutrino interactions in the CDHS apparatus[35], at a rate consistent with π/K decay contamination of dimuon events. The small pair masses and transverse momenta in event 851-5726 favor such an interpretation. The size of the corresponding dimuon sample places a bound on the probability of π/K decay into a detectable muon ($\gtrsim$ 10 GeV). This probability is less than 10^{-4} per hadron shower in the apparatus.

Five-muon events

No 5-muon final state (or 4-muon final state with other than μ or ν_μ incident) has been reported by any previous experiment. It is natural to try to interpret events 1208-3386 and 851-11418 as QED phenomena ("muon pentads"). Their negligible hadronic and missing energies support such an interpretation. Event 1208-3386 possesses values of Q^2, pair masses and daughter transverse momenta typical of muon tridents, which are more abundant by a factor consistent with α^{-2}. However, event 851-11418, shown in Fig. 18, has kinematic properties which are puzzling. To explore these properties, all lowest-order QED diagrams have been examined. One diagram has been found to minimize the product of the denominators in the lepton and photon propagators. It is a Bethe-Heitler-like graph with the incident muon scattered into track 2 and coupled to track 5, and the target coupled to track 3. Tracks 4 and 6 form a pair radiated by track 5. The unseen $p_\perp$ is 1.8±0.4; for the above choice of scattered muon, Q^2 is 3.5±0.6, and the daughter (unscattered) muons have a combined mass M_{3456}=3.5±0.3. Of the muon tridents observed in the same data set, fewer than 200 have Q^2>2.5 and combined daughter muon mass >2.8; fewer than 20% of these have unseen $p_\perp$>1.4. A parent sample of that size would not be expected to yield one event with an additional energetic muon pair. The event requires a more plausible explanation.

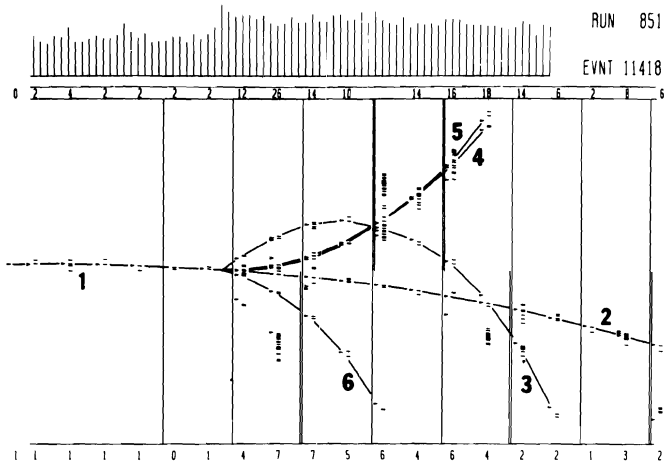

FIG. 18. Plane view of five-muon event #851-11418. Superimposed digits are the track numbers mentioned in the text and Table 3. Tracks 4 and 5 are well separated in the elevation view (not shown). Typically, in each interstice between modules a track registers in a proportional chamber (left tic) and drift chamber (right tic closest to left tic). The drift chambers are noisier due to their longer livetime. Short vertical lines at the top are calorimeter counter pulse heights. Long vertical lines are projections of trigger counters which were tagged. Heavy broken lines are tracings of the computer-reconstructed trajectories.

Four-muon event interpreted as $b\bar{b}$ production with $\bar{b}\to\psi X$, $b\to\mu^-X$.

One neutrino-induced four-lepton final state has been observed by each of three groups: CDHS[36], BFHSW[37], and HPWFOR[38]. The respective authors expect $\sim$1/5 of an event as background in the CDHS and HPWFOR samples, and $\sim10^{-3}$ events in the BFHSW sample. The kinematics of muon-induced 4μ event 1191-5809 are summarized in Table 3 and compared with those of the neutrino-induced events in Table 4. The muon-induced event is qualitatively different from the others. The softest lepton has at least 4× the energy and the lightest $\mu^+\mu^-$ daughter pair has at least 4× the mass of any neutrino-induced counterpart.

A relatively model-independent limit can be placed on this event's most obvious potential background -- single muon production due to any process, in *random* association with $\mu^+\mu^-$ pair production due to any process within the same diagram. Choosing the leading secondary (track 2) as the scattered muon produces the smallest Q^2 and determines the virtual-photon direction represented by the central axis of Fig. 19. The $\mu^+\mu^-$ pair is interpreted as that formed by tracks 3 and 4, because it is no more massive than that formed by tracks 3 and 5, but has only half the transverse momentum. Let

N_0 = calculated no. of μ scatters with y>1/2 corresponding to the sensitivity of this data set.

N_1 = observed no. of 2μ final states in which y>1/2 and the nonleading μ has E>15 and $p_\perp$>1.7 (Fig. 19).

N_2 = observed no. of 3μ final states with E_{pair}>30, (ν-E_{pair})>100, and M_{pair}>2.75.

Table 4. Comparison of event 1191-5809 to published neutrino-induced 4-lepton events.

Group	Final state leptons	Smallest lepton energy (GeV)	Smallest $\mu^+\mu^-$ or e^+e^- pair mass $(GeV/c)^2$
CDHS	$\mu^+\mu^-\mu^+\mu^-$	4.5	0.4
BFHSW	$\mu^+e^-e^+e^-$	0.9	0.8
HWPFOR	$\mu^-\mu^+\mu^+\mu^?$	3.0	0.5
This experiment	$\mu^+\mu^+\mu^-\mu^-$	18.3	3.0

The number of N_B of background events is then

$$N_B < \varepsilon_B N_1 N_2/(\varepsilon_1\varepsilon_2 N_0),$$

where the ε's are detection efficiencies. Using $\varepsilon_B/\varepsilon_1\varepsilon_2<10$, $N_1<200$, $N_2<13$, and $N_0=3.7\times10^7$, one obtains $N_B<7\times10^{-4}$.

The interpretation of event 1191-5809 as an example of

$$\mu_1^+ N \to \mu_2^+ b\bar{b} X \text{ (diffractive)};$$

$$\bar{b} \to \psi X \to \mu_3^+\mu_4^- X ;$$

$$b \to \mu_5^-\bar{\nu}_\mu X$$

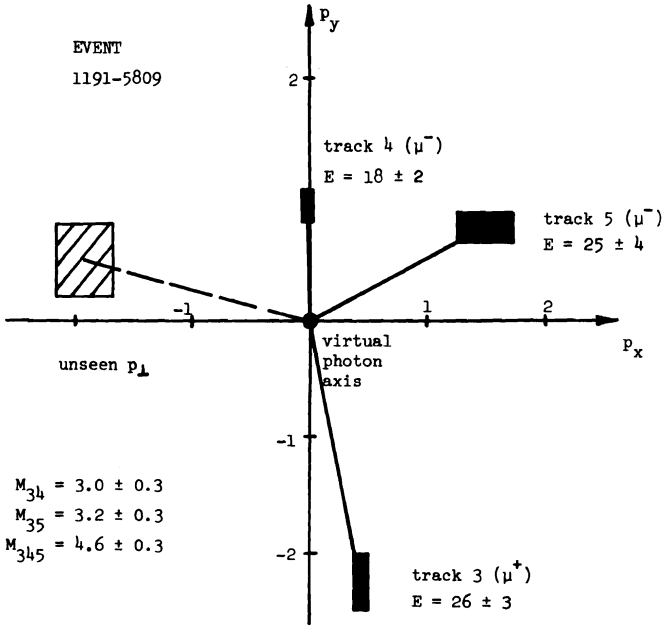

FIG. 19. Momenta transverse to the direction of the virtual photon in event 1191-5809. Dark boxes: secondary muons other than the scattered (spectator) muon. Hatched box: unseen transverse momentum carried off by neutrinos and/or hadrons. Box sizes indicate measurement error. Tracks 3 and 4 are interpreted as products of $\psi \to \mu\mu$ decay where the ψ arises from $\bar{b}$ decay; track 5 is interpreted as the μ^- from semileptonic b decay. Incident and scattered muon tracks are not shown.

[muon subscripts refer to track numbers] is motivated by the prediction by Fritzsch[39] and subsequent possible observation by the Saclay-Imperial College-Southampton-Indiana (SISI) group[40] of the decay mode $B\to\psi K(n\pi)$, where B is a meson containing the b quark. Specifically, SISI reports the observation in the CERN-SPS WA-11 spectrometer of narrow enhancements at 5.3 GeV/c^2 in the $\psi K^+\pi^-$ and $\psi K^0\pi^\pm$ mass spectra produced by 150-175 GeV $\pi^- N$ interactions. The experimenters estimate $\sigma(\pi^- N\to B\bar{B}X)\times BR(B\to\psi K\pi)\sim 2$ nb.

There are eight arguments favoring the hypothesis of $b\bar{b}$ production with $\bar{b}\to\psi$ and $b\to\mu$ decay as an explanation for event 1191-5809.

(1) This candidate is our only four-muon event satisfying the rare-event analysis requirements detailed above. In no way is it selected to satisfy any kinematic criterion other than the observation of four muons in the final state.

(2) The mass of $\mu_3^+\mu_4^-$ (henceforth called ψ_{34}) is 3.05 ± 0.26 GeV/c^2. In contrast, only 1.4% of the muon-pair continuum produced by muons and detected in our apparatus comes within one standard deviation (9%) of the ψ mass.

(3) The event has ν=158 GeV. From our measurements of the ν-dependence of ψ production, we estimate that nearly all detectable $b\bar{b}$ production in our apparatus has $130<\nu<190$ GeV. Only 1/4 of ψ production occupies this range.

(4) The inelasticity of this event is $k \equiv 1 - E_\psi/\nu = 0.72$. If produced at rest in the c.m. of a diffractively-produced system of B and $\bar{B}$ with small relative velocity, the expected inelasticity is $1 - m_\psi/2m_B = 0.71$. In contrast, only 4% of all events containing a ψ in the final state have $k > 0.45$.

(5) If emitted at 90° to the virtual photon direction in some frame, ψ_{34} requires that frame to have γ_{34}=13.2, while μ_5^- (track 5) requires γ_5=14.9. A parent system with energy equal to ν and with $\gamma = 1/2(\gamma_{34}+\gamma_5)$ has a mass of 11.2 GeV, very close to twice the B mass.

(6) In a frame moving with $\gamma=\nu/2M_B$ in the virtual-photon direction, the muon μ_5^- which is interpreted as arising from $b \to \mu_5^-\bar{\nu}_\mu X$ has energy 1.7 GeV. Thrice the peak energy of the electron spectrum from $D \to Ke\nu$ ($K^*e\nu$) is equal to 1.7 (1.3) GeV. In contrast, only 3.4% of singly produced "extra" muons in this experiment have $p_\perp > 1.4$ GeV/c.

(7) If, in the same frame as in (6) above, ψ_{34} is the decay product of $\bar{B}$ at rest, it recoils against an invariant mass of 1.25 GeV/c^2. This is well within the range $1.1 < m_{K\pi} < 1.8$ GeV/c^2 mentioned by the SISI group.

(8) The observed event rate is in good agreement with our estimate based on the SISI cross-section. Briefly, use of ψ-production measurements by 150 GeV[41] and 16 GeV[42] π^- together with our measurements of ψ muoproduction lead to the estimate that 165-GeV π^- are $\sim$150× more efficient at producing ψ's than are 209-GeV muons. If each beam energy is reduced by $(m_\psi/m_T)^2$ the conclusion is unchanged. Defining

$$A \approx 150^{-1} \text{ (above)}\times(e_b/e_c)^2 \approx 600^{-1},$$

$$C = \frac{\Gamma(B\to\psi X)}{\Gamma(B\to\psi K\pi)} \approx \frac{\Gamma(K^*(1430)\to \text{all})}{\Gamma(K^*(1430)\to K\pi)} = 2,$$

$$E = BR\,(B\to\mu X)\times BR\,(\psi\to\mu\mu) \approx 0.007,$$

we estimate

$$\sigma \times BR\ (\mu N \to B\bar{B}X;\ \bar{B} \to \psi X \to \mu^+\mu^- X;\ \bar{B} \to \mu X) \approx$$

$$\approx 2\ \text{nb} \times ACE \approx 5 \times 10^{-38}\ \text{cm}^2.$$

In a ≈0.3-event/10^{-38} cm^2 exposure one expects 1.5 events from this process. In contrast, we know of no background mechanism which could be responsible for more than 10^{-3} such events.

We conclude that event 1191-5809 would be truly surprising if it were explained by a mechanism *other than* one similar to that which we have proposed.

Using $BR\ (b \to \mu X) = 0.1$, the assumption that (coincidentally) $BR\ (T \to \mu\mu) \approx BR\ (b \to \psi X)$, and the 90%-confidence limit $\sigma(\mu N \to TX) < 0.6 \times 10^{-38}$ cm^2 reported to this conference by Benvenuti[11], the above interpretation of event 1191-5809 results in the lower limit

$$\frac{\sigma\ (\mu N \to b\bar{b}X)}{\sigma\ (\mu N \to TX)} > 50\text{-}200\ (90\%\ \text{conf.}),$$

where the range arises from the present crude estimate of detection efficiency for 4μ final states. This limit is ∿1/2 order of magnitude higher than our earliest measurement of the $c\bar{c}/\psi$ production ratio. As a very early candidate for interpretation as associated production and decay of b and $\bar{b}$, the 4μ event may demonstrate conservation of the quantum number associated with these heavy quarks.

We appreciate the efforts of Fermilab and its Neutrino Department which made possible a very successful run. One of us (M.S.) thanks R. Cahn, M. Chanowitz, and M. Suzuki for discussions particularly on ≥4μ final states. We take this opportunity to acknowledge the magnificent support received from our engineering and technical groups: T. Ahmadvand, W. Baldock, F. Goozen, K. Lucas, T. Nuzum, T. Weber and coworkers at LBL; G. Hale, B. Hanna, W. Nestander and coworkers at Fermilab; C. Bopp, A. David, H. Edwards, M. Isaila and coworkers at Princeton. This work was supported by the High Energy Physics Division of the U.S. Department of Energy under contract Nos. W-7405-Eng-48, EY-76-C-02-3072, and EY-76-C-02-3000.

---

[1]Y. Watanabe, L.N. Hand, S. Herb, A. Russell, C. Chang, K.W. Chen, D.J. Fox, A. Kotlewski, P.F. Kunz, S.C. Loken, M. Strovink, and W. Vernon, Phys. Rev. Lett. 35, 898 (1975); C. Chang, K.W. Chen, D.J. Fox, A. Kotlewski, P.F. Kunz, L.N. Hand, S. Herb, A. Russell, Y. Watanabe, S.C. Loken, M. Strovink, and W. Vernon, Phys. Rev. Lett. 35, 901 (1975).

[2]R. Cester, C.M. Hoffman, M. Strovink, and F.C. Shoemaker, Fermilab Proposal 203 (1973, unpublished).

[3]G. Gollin, M.V. Isaila, F.C. Shoemaker, and P. Surko, IEEE Trans. Nuc. Sci. NS-26, 59 (1979).

[4]H.L. Anderson *et al.*, FERMILAB-Pub-79/30-EXP (submitted to Phys. Rev. D), Table X, last column (1979).

[5]A. Bodek *et al.*, SLAC-PUB-2248 (submitted to Phys. Rev. D), Fig. 31(f) (1979). See also Ref. 13.

[6]J.G.H. deGroot *et al.*, Z. Physik C1, 143 (1979).

[7]Crudely, we assumed E_0=19.5 GeV for SLAC-MIT data (Ref. 13) and y = max(ν/190, min(ν/(ν+7), 0.42)) for CDHS data (Ref. 6). The unfortunate lack of precision in these choices is justified only by the small size of the corrections involved.

[8]A.J. Buras and K.J.F. Gaemers, Nucl. Phys. B132, 249 (1979). We have benefited from conversations with Dr. Buras and from the use of the computer code which generated the fits in the publication cited above.

[9]For example, in the Buras-Gaemers fit (Ref. 8) with Λ=0.3, between $10 < Q^2 < 150$ $\partial \ell n F_2/\partial s$ is confined within the range -.38 to -.52 (x=.25), -.56 to -.66 (x=.35), -.73 to -.82 (x=.45), -.92 to -1.00 (x=.55).

[10]H. Stier, Invited Paper presented at this Symposium.

[11]A. Benvenuti, Invited Paper presented at this Symposium.

[12]Due to the extremely small statistical errors, in some regions the ∿10% differences between 209-GeV and 90-GeV structure functions enlarged the best fit χ^2. In each x range we allowed crudely for these effects by adding a fixed error in quadrature with the statistical error of each data point. The extra error was large enough to make the straight-line fit at least 30% probable. The errors added were zero, except for x=0.15 (1%), and x=0.25, 0.35, and 0.45 (4%).

[13]We have used a compilation of the following data made by W.B. Atwood with our very slight interpolation to our x-region centers: M.D. Mestayer, SLAC-Report No. 214 (Aug. 1978) (Ph.D. Dissertation); J.S. Poucher *et al.*, Phys. Rev. Lett. 32, 118 (1974), and SLAC-PUB-1309 (unpublished); E.M. Riordan *et al.*, Phys. Rev. Lett. 33, 561 (1974); E.M. Riordan, MIT LNS Report No. COO-3069-176, MIT Ph.D. Thesis (unpublished); W.B. Atwood *et al.*, Phys. Lett. 64B, 497 (1976); W.B. Atwood, SLAC Report No. SLAC-185, Stanford Ph.D. Thesis, 1975 (unpublished); A. Bodek *et al.*, SLAC-PUB-2248 (1979), submitted to Phys. Rev. D; A. Bodek, MIT LNS Report No. COO-3069-116, MIT Ph.D. Thesis (unpublished).

[14]A. Para, Invited Paper presented at this Symposium, and private communication. We are grateful to Dr. Para and Dr. H. Geweniger for their patience and care in explaining to us the CDHS analysis procedures.

[15]Using the method described in Ref. 12, it was necessary only to add in quadrature with SLAC-MIT points a 2% error at x=.35 and a 1% error at x=.45. The fits to CDHS data all enjoyed a high level of statistical confidence.

[16]M.D. Mestayer (Ref. 13), Fig. IV-4(a), scaling variable=x.

[17]A.R. Clark, K.J. Johnson, L.T. Kerth, S.C. Loken, T.W. Markiewicz, P.D. Meyers, W.H. Smith, M. Strovink, W.A. Wenzel, R.P. Johnson, C. Moore, M. Mugge, R.E. Shafer, G.D. Gollin, F.C. Shoemaker, and P. Surko, Phys. Rev. Lett. 43, 189 (1979), and Paper #57 contributed to this Symposium.

[18]M. Strovink, "First Results from the Berkeley-Fermilab-Princeton Multimuon Spectrometer", in *Probing Hadrons with Leptons* (Proceedings of the Seminar on Probing Hadrons with Leptons, Erice, Trapani, Sicily, March 13-21, 1979), edited by G. Preparata and J.J. Aubert (Plenum, New York) (1979), and LBL-9234, and Paper #58 contributed to this Symposium.

[19]B. Knapp *et al.*, Phys. Rev. Lett. 34, 1040 (1975); W.Y. Lee, in Proc. Int. Symp. on Lepton and Photon Interactions at High Energies (DESY, Hamburg, 1977); M. Binkley, private communication.

[20]T. Nash *et al.*, Phys. Rev. Lett. 36, 1233 (1976).

[21]U. Camerini *et al.*, Phys. Rev. Lett. 35, 483 (1975).

[22]B. Gittelman *et al.*, Phys. Rev. Lett. 36, 1616 (1975).

[23]M. Glück and E. Reya, Phys. Lett. 79B, 453 (1978); M. Glück and E. Reya, DESY preprint 79/05 (1979). In Fig. 9 we have multiplied their result for σ by 2.4 to obtain $d\sigma/dt$ (t=0).

[24]P. Joos *et al.*, Nucl. Phys. B113, 53 (1976).

[25]R. Dixon *et al.*, Phys. Rev. Lett. 39, 516 (1977).

[26]W.R. Francis *et al.*, Phys. Rev. Lett. 38, 633 (1977).

[27]K. Schilling and G. Wolf, Nucl. Phys. B61, 381 (1973).

[28]V. Barger, W.Y. Keung, and R.J.N. Phillips, Phys. Rev. D20, 630 (1979), and Paper #81 contributed to this Symposium.
[29]J.P. Leveille and T. Weiler, Nucl. Phys. B147, 147 (1979); J.P. Leveille and T. Weiler, Wisconsin/Northeastern preprint COO-881-101/NUB #2398 (1979).
[30]T. Weiler, speculation privately communicated.
[31]The equation of this line is $p_\perp = \max(1.4,\ 3.8-0.348\sqrt{Q^2})$.
[32]A. Pais and S.B. Treiman, Phys. Rev. Lett. 35, 1206 (1975).
[33]The two events having a third muon track candidate are the two events with missing energy closest to zero.
[34]C. Prescott, Invited Paper presented at this Symposium.
[35]T. Hansl *et al.*, Phys. Lett. 77B, 114 (1978).
[36]M. Holder *et al.*, Phys. Lett. 73B, 105 (1978).
[37]R.J. Loveless *et al.*, Phys. Lett. 78B, 505 (1978).
[38]A. Benvenuti *et al.*, Phys. Rev. Lett. 42, 1024 (1979).
[39]H. Fritzsch, CERN preprint TH2648 (March 1979). See also H. Fritzsch and K. Streng, Phys. Lett 78B, 447 (1979); H. Fritzsch, CERN preprint TH2703 (July 1979).
[40]R. Barate *et al.*, Saclay preprint D Ph P E 79-17 (1979); presented in behalf of the SISI group by D. Treille at the European Physical Society Conference on High Energy Physics, Geneva, June 27-July 4, 1979.
[41]K.J. Anderson *et al.*, Phys. Rev. Lett. 37, 799 (1976).
[42]J. LeBritton *et al.*, Phys. Lett. 81B, 401 (1979).

DISCUSSION

H.L. Anderson, University of Chicago: How did you choose the parameters for the Buras and Gaemers fit?

M. Strovink: We inherited Buras and Gaemers' computer code, ran it and reproduced the numbers they published. The Buras-Gaemers curves I showed are not a fit to the most current data.

M. Tannenbaum, Rockefeller University: What does the τ lepton do to your multi-lepton sample? If it is a lepton you can calculate everything about it. How many events would you expect, and so on?

Strovink: When both τ's decay muonically they should appear as a component of the elastic trimuon signal which exhibits considerable missing energy. We have not completed a quantitative calculation for τ pair production or, for that matter, for μ pair production.

P. Langacker, University of Pennsylvania: It appeared to me that your single muon data did not show strong signs of scaling violation. Would you care to comment?

Strovink: There is a difference between looking at the whole picture and looking at part of the picture. If you take the upper half of the range in $\log(\log Q^2)$ that we cover, then you do not see much scale-noninvariance -- some, but not much. In order to make strong statements on the basis of those data alone, you would have to assume that the 1-2% statistical errors are the only errors. At the present stage of our analysis, that's nonsense. The whole picture is given by the combination of our 90-GeV and 209-GeV data. Over the full range in $\log(\log Q^2)$ there is a clear decrease of F_2 with rising Q^2, particularly for x above 0.3.